Eur. Phys. J. A (2012) **48**: 64
DOI 10.1140/epja/i2012-12064-y

THE EUROPEAN PHYSICAL JOURNAL A

Regular Article – Experimental Physics

Inclusive dielectron spectra in p+p collisions at 3.5 GeV kinetic beam energy

HADES Collaboration

G. Agakishiev[6], A. Balanda[3], D. Belver[17], A. Belyaev[6], A. Blanco[2], M. Böhmer[9], J.L. Boyard[15], P. Cabanelas[17], E. Castro[17], J.C. Chen[8], S. Chernenko[6], T. Christ[9], M. Destefanis[10], F. Dohrmann[5], A. Dybczak[3], E. Epple[8], L. Fabbietti[8], O. Fateev[6], P. Finocchiaro[1], P. Fonte[2,a], J. Friese[9], I. Fröhlich[7], T. Galatyuk[7,b], J.A. Garzón[17], R. Gernhäuser[9], C. Gilardi[10], M. Golubeva[12], D. González-Díaz[c], F. Guber[12], M. Gumberidze[15], T. Heinz[4], T. Hennino[15], R. Holzmann[4], A. Ierusalimov[6], I. Iori[11,d], A. Ivashkin[12], M. Jurkovic[9], B. Kämpfer[5,e], K. Kanaki[5], T. Karavicheva[12], I. Koenig[4], W. Koenig[4], B. W. Kolb[4], R. Kotte[5], A. Krása[16], F. Krizek[16], R. Krücken[9], H. Kuc[3,15], W. Kühn[10], A. Kugler[16], A. Kurepin[12], R. Lalik[8], S. Lang[4], J.S. Lange[10], K. Lapidus[8], T. Liu[15], L. Lopes[2], M. Lorenz[7], L. Maier[9], A. Mangiarotti[2], J. Markert[7], V. Metag[10], B. Michalska[3], J. Michel[7], E. Morinière[15], J. Mousa[14], C. Müntz[7], L. Naumann[5], J. Otwinowski[3], Y. C. Pachmayer[7], M. Palka[7], Y. Parpottas[14,13], V. Pechenov[4], O. Pechenova[7], J. Pietraszko[7], W. Przygoda[3], B. Ramstein[15], A. Reshetin[12], A. Rustamov[7,f], A. Sadovsky[12], P. Salabura[3], A. Schmah[g], E. Schwab[4], J. Siebenson[8], Yu.G. Sobolev[16], S. Spataro[h], B. Spruck[10], H. Ströbele[7], J. Stroth[7,4], C. Sturm[4], A. Tarantola[7], K. Teilab[7], P. Tlusty[16], M. Traxler[4], R. Trebacz[3], H. Tsertos[14], V. Wagner[16], M. Weber[9], C. Wendisch[5], J. Wüstenfeld[5], S. Yurevich[4], and Y. Zanevsky[6]

[1] Istituto Nazionale di Fisica Nucleare - Laboratori Nazionali del Sud, 95125 Catania, Italy
[2] LIP-Laboratório de Instrumentação e Física Experimental de Partículas, 3004-516 Coimbra, Portugal
[3] Smoluchowski Institute of Physics, Jagiellonian University of Cracow, 30-059 Kraków, Poland
[4] GSI Helmholtzzentrum für Schwerionenforschung GmbH, 64291 Darmstadt, Germany
[5] Institut für Strahlenphysik, Helmholtz-Zentrum Dresden-Rossendorf, 01314 Dresden, Germany
[6] Joint Institute of Nuclear Research, 141980 Dubna, Russia
[7] Institut für Kernphysik, Goethe-Universität, 60438 Frankfurt, Germany
[8] Excellence Cluster "Origin and Structure of the Universe", 85748 Garching, Germany
[9] Physik Department E12, Technische Universität München, 85748 Garching, Germany
[10] II.Physikalisches Institut, Justus Liebig Universität Giessen, 35392 Giessen, Germany
[11] Istituto Nazionale di Fisica Nucleare, Sezione di Milano, 20133 Milano, Italy
[12] Institute for Nuclear Research, Russian Academy of Science, 117312 Moscow, Russia

[a] *Also at:* ISEC Coimbra, Coimbra, Portugal.
[b] *Also at:* ExtreMe Matter Institute EMMI, 64291 Darmstadt, Germany.
[c] *Also at:* Technische Universität Darmstadt, Darmstadt, Germany.
[d] *Also at:* Dipartimento di Fisica, Università di Milano, 20133 Milano, Italy.
[e] *Also at:* Technische Universität Dresden, 01062 Dresden, Germany.
[f] e-mail: `Rustamov@Physik.uni-frankfurt.de` (corresponding author)
[g] *Also:* at Lawrence Berkeley National Laboratory, Berkeley, USA.
[h] *Also at:* Dipartimento di Fisica Generale and INFN, Università di Torino, 10125 Torino, Italy.

[13] Frederick University, 1036 Nicosia, Cyprus
[14] Department of Physics, University of Cyprus, 1678 Nicosia, Cyprus
[15] Institut de Physique Nucléaire (UMR 8608), CNRS/IN2P3 - Université Paris Sud, F-91406 Orsay Cedex, France
[16] Nuclear Physics Institute, Academy of Sciences of Czech Republic, 25068 Rez, Czech Republic
[17] Departamento de Física de Partículas, Univ. de Santiago de Compostela, 15706 Santiago de Compostela, Spain

Received: 18 December 2011 / Revised: 8 March 2012
Published online: 11 May 2012
© The Author(s) 2012. This article is published with open access at Springerlink.com
Communicated by M. Guidal

Abstract. We present the inclusive invariant mass, transverse momentum and rapidity distributions of dielectrons (e^+e^- pairs) in p+p interactions at 3.5 GeV beam kinetic energy. In the vector meson mass region, a distinct peak corresponding to direct ω decays is reconstructed with a 2% mass resolution. The data is compared to predictions from three model calculations. Due to the large acceptance of the HADES apparatus for e^+e^- invariant masses above 0.2 GeV/c^2 and for transverse pair momenta $p_t < 1$ GeV/c, acceptance corrections are, to a large extent, model independent. This allows us to extract from dielectron data for the first time at this energy the inclusive production cross-sections for light vector mesons. Inclusive production cross-sections for π^0 and η mesons are also reported. The obtained results will serve as an important reference for the study of vector meson production in proton-nucleus and heavy-ion collisions. Furthermore, using this data, an improved value for the upper bound of the branching ratio for direct η decays into the electron-positron channel is obtained.

1 Introduction

The High Acceptance Di-Electron Spectrometer (HADES) [1] is operated at the GSI Helmholtzzentrum für Schwerionenforschung in Darmstadt, Germany. One of the main physics goals of HADES is to investigate spectral modifications of light vector mesons in strongly interacting matter. The question is how the low-energy QCD spectrum, which is experimentally known in the vacuum in terms of hadron spectra, will change when this vacuum is heated and filled up with color charges. Spectral modifications of hadrons (encoded, *e.g.*, by changes of their masses and decay widths) in hot and/or dense matter are often discussed in the context of the restoration of the broken chiral symmetry. Detailed investigations, however, reveal that the link between hadron properties and QCD symmetries is not as direct as originally envisaged [2,3].

In order to search for in-medium effects, results on electron-positron invariant-mass spectra from proton-induced reactions on nuclei and from heavy-ion collisions should be compared systematically and complemented with insights gained from photo-induced reactions. The interpretation of nuclear data requires a firm knowledge of the corresponding data from proton-proton (p+p) collisions. These investigations are also important for transport model calculations, as the dilepton spectra from elementary interactions serve as input to these codes. Given this motivation, the HADES Collaboration has set up an experimental program to measure dilepton spectra in elementary collisions. First results were discussed in [4]. Here we present the inclusive dielectron spectra measured in p+p collisions at 3.5 GeV kinetic beam energy.

At this energy the dominant mechanisms for hadron production are still controversially discussed and inclusive production cross-sections are not yet measured. In fact, various production scenarios are assumed in different transport codes: While in HSD[1] [5] and GiBUU[2] [6] hadrons are produced at this beam energy through string fragmentation [7], in UrQMD[3] [8] the decays of nucleon resonances are the sources of final-state particles, in particular of mesons.

Another uncertainty concerns the Dalitz decays of baryon resonances ($R \to N\mathrm{e}^+\mathrm{e}^-$). Here two different aspects are a matter of discussion. First, the R Dalitz decay process, *i.e.* its decay into a nucleon and a massive photon with the subsequent decay of the latter into a dielectron, depends on the electromagnetic structure of the N-R transition vertex. In case of the $\Delta(1232)$ resonance this transition vertex depends on three independent helicity amplitudes corresponding to three helicity states of the massive photon and two of the nucleon. Equivalently, one can describe this vertex by three independent transition form factors built up from the helicity amplitudes. In this decay process, the squared four-momentum of the virtual photon equals the squared invariant mass of the lepton pair and therefore is a positive quantity. Such a photon transfers energy and is said to be a time-like photon[4]. There are also other processes (*e.g.*, pion electro-production) where the virtual photon transfers momentum, but not energy, and is then referred to as space-like. While in case of space-like photons the above-mentioned transition form factors have been measured in quite a wide range of four-momentum transfers, for time-like photons their mass dependence is not settled yet. The mass dependence of the form factors is usually modeled within the Vector Meson Dominance (VMD) model. In this picture, the virtual photon couples to the nucleon through intermediate vector meson (ρ, ω, ϕ) states. However, it is known that the standard VMD model of Sakurai [9,10] significantly overestimates the radiative ($R \to N\gamma$) branching ratios once the coupling constant is extracted from the corresponding mesonic decays. The modified VMD model of Kroll *et al.* [11] allows to fix the ρN and γN coupling constants independently. The asymptotic behavior of the transition form factors predicted by both models disagrees, however, with the outcome of quark counting rules [12]. On the other hand, the authors of [12] demonstrated in their framework of extended VMD that the incorporation of higher vector meson states resolves the problem between photon and ρ meson branchings of the nucleon resonances. Yet another VMD model variant for the nucleon form factors was proposed by Iachello [13]. It describes simultaneously the nucleon space-like and time-like form factors as well as space-like N-Δ transition form factors [14,15].

A second aspect of resonance decays to consider is the parametrization of the mass-dependent resonance width. Various prescriptions are used in model calculations (for details, see sect. 3 and [16]) which differ at high resonance masses. As a consequence, the resulting dielectron yield from the resonance Dalitz decays has a large uncertainty, as shown for $\Delta(1232)$ in [16].

Our precision data offer, hence, a unique possibility to address the above-mentioned problems.

This paper is organized as follows. After giving detailed information about the collected data and analysis chain in sect. 2, we report, in sect. 3, on a comparison of the data with model calculations. The sensitivity of the data to the N-Δ electromagnetic transition vertex is also discussed in this section. The extraction of π^0, η, $\Delta(1232)$, ρ and ω cross-sections is discussed in sect. 4. The data allow to improve the upper bound of the direct $\eta \to \mathrm{e}^+\mathrm{e}^-$ decay, as discussed in sect. 5.

2 The data

In the experiment (see [1] for a detailed description of HADES), a proton beam of 10^7 particles/s with a kinetic energy of 3.5 GeV was incident on a 4.4 cm long liquid-hydrogen target [17]. The data readout was started upon

[1] Hadron-String Dynamics.

[2] Giessen Boltzmann-Uehling-Uhlenbeck project.

[3] Ultrarelativistic Quantum Molecular Dynamics.

[4] We use the following convention of the squared 4-momenta: $p^2 = p^\mu(E,\boldsymbol{p})p_\mu(E,-\boldsymbol{p}) = E^2 - |\boldsymbol{p}|^2$, *i.e.*, the positive p^2 is called time-like, and the negative p^2 is, correspondingly, space-like.

a first-level trigger (LVL1) decision. Depending on the reaction channel of interest, two different settings of the LVL1 trigger were required: i) a charged-particle multiplicity MULT ≥ 3 to enhance inclusive dielectron production and ii) MULT ≥ 2 with hits in opposite sectors ($\Delta\phi = 180^\circ \pm 60^\circ$) of the time-of-flight detectors to enrich elastic p+p events used for the absolute normalization of the dielectron data. The LVL1 was followed by a second-level trigger (LVL2) requesting at least one electron candidate recognized in the Ring-Imaging Cherenkov Detector (RICH) and time-of-flight/pre-shower detectors [1]. All events with positive LVL2 trigger decision and every third LVL1 event, irrespective of the LVL2 decision, were recorded, yielding a total of 1.17×10^9 events.

The identified single-electron and single-positron tracks were combined into opposite-sign pairs. However, many of these pairs represent combinatorial background (CB) which is mostly due to uncorrelated pairs from multi-pion Dalitz decays and correlated ones from $\pi^0 \to \gamma\gamma$ accompanied by photon conversion in the detector material and/or from Dalitz decays. The combinatorial background was reduced by using an opening angle cut of $\alpha_{ee} > 9^\circ$ between the reconstructed lepton tracks and a condition on quality criteria of the track-fitting algorithm [1]. In addition a momentum cut of $0.08 < p$ [GeV/c] < 2 for each lepton was applied. The combinatorial background was formed from the sum of the reconstructed like-sign invariant-mass distributions, $\mathrm{d}N^{++}/\mathrm{d}M_{ee}$ and $\mathrm{d}N^{--}/\mathrm{d}M_{ee}$. The like-sign pairs were subjected to the same selection criteria as the unlike-sign ones. Both, the unlike-sign invariant-mass distribution and the CB, were corrected for the detector and reconstruction inefficiencies on a pair-by-pair basis, defined as the product of single-lepton efficiencies deduced from dedicated Monte-Carlo events embedded into real events [1,18,19]. The geometrical pair acceptance (the acceptance matrix) of the HADES detector was obtained in a similar way from single-lepton acceptances defined as a function of the lepton momentum, polar and azimuthal emission angles [1].

The final signal pair distribution inside the geometrical acceptance of the HADES, shown in fig. 1, is the result of a subtraction of the CB from the unlike-sign invariant-mass distribution. Both spectra are normalized to $N_{el}^{acc}/\sigma_{el}^{acc}$, where N_{el}^{acc} and σ_{el}^{acc} denote the measured yield of the p+p elastic scattering and the differential elastic cross-section [20] inside the acceptance of HADES, respectively.

The low-mass region of the spectrum in fig. 1 is dominated by Dalitz decays of neutral mesons (π^0, η, ω), as well as by the Dalitz decay of the $\Delta(1232)$ resonance (see below). The evident peak around the pole mass of the ω meson corresponds to its direct decay into $\mathrm{e}^+\mathrm{e}^-$ pairs. However, this mass range contains also pairs stemming from the direct decays of the ρ meson. In total, 6.1×10^4 signal pairs, 5.4×10^4 of them in the region below 0.15 GeV/c^2, were reconstructed. The number of pairs in the mass range between 0.71 GeV/c^2 and 0.81 GeV/c^2, which corresponds to the $\pm 3\sigma$ interval around the reconstructed ω peak, amounts to 260. In the inset of fig. 1, the ω peak is shown on a linear scale. In order to estimate the mass resolution,

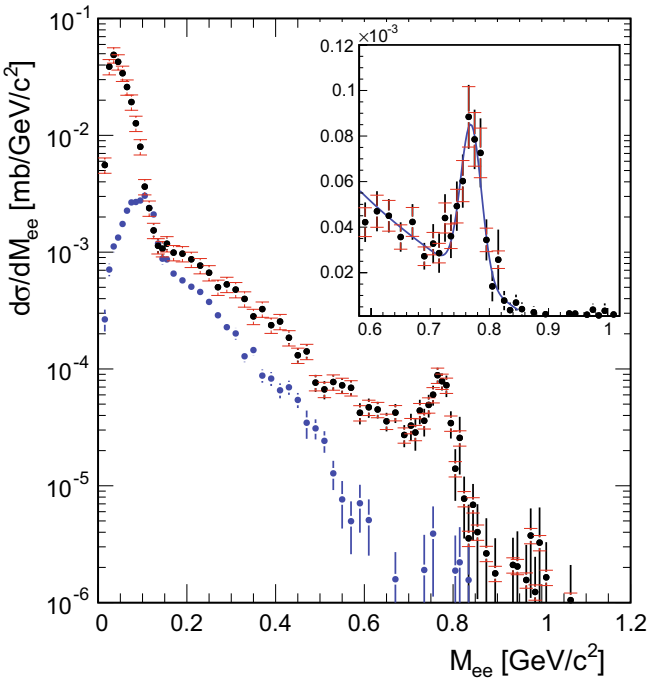

Fig. 1. (Color online) Efficiency corrected inclusive invariant-mass distribution of dielectrons inside the geometrical acceptance of HADES of signal (black dots) $\mathrm{e}^+\mathrm{e}^-$ pairs after combinatorial background (blue dots) subtraction for p(3.5 GeV)+p collisions. In the right upper part of the figure the ω meson region is shown on a linear scale. The data are normalized to the simultaneously measured p+p elastic events.

this peak was fitted with a Gaussian distribution plus a polynomial for the underlying continuum. The obtained mass resolution, σ/M_{pole}^{ω}, is about 2%.

3 Comparison to three models

3.1 PYTHIA+PLUTO, UrQMD, HSD

For better understanding of the inclusive hadron production in 3.5 GeV p+p interactions, we compare in this section the experimentally measured distributions to the results from the PYTHIA [21], UrQMD [22,8] and HSD [5, 23] event generators.

PYTHIA, as well as HSD at this energy, uses a Monte Carlo realization of the Lund string fragmentation model, where the assumption of a linear confinement potential between the quark and antiquark is taken as a starting point. Although the latter is usually used to describe the multi-particle production in the high-energy regime, it was successfully applied, with some additional adjustments, called tunes, to reproduce the experimental data at low energies. In particular, since PYTHIA is not predictive in assigning the spin to the newly created quark and anti-quark pairs from two adjacent string break-ups, it has a tunable parameter which can be adjusted in order to get

Table 1. Tuned values of PYTHIA parameters used in our simulation. Detailed descriptions of these parameters are given in PYTHIA documentation [21].

	Tuned value	Default value
PARJ(11)	0.15 [25]	0.5
PARJ(25)	0.63 [25]	1.0
PARP(91)	0.44	2.0

vector meson multiplicities in accordance with our measured vector meson yields. Recently such tunes have been obtained by the Giessen group, in particular for the p+p data at 3.5 GeV [24,25]. Tuned values of PYTHIA parameters used in our simulation are listed in table 1.

A large fraction of the hadrons produced by fragmentation are unstable and subsequently decay into final states. We do not let the particles decay directly inside PYTHIA, but rather using the PLUTO [26] code. The input information obtained from PYTHIA consists thus of the particle multiplicities and their four-momenta.

The simulated dielectron spectra (referred to as the cocktail) can be expressed as the incoherent sum over various sources of dielectrons, such as Dalitz decays of the pseudoscalar mesons π^0 and η, Dalitz decay of the vector meson ω, Dalitz decay of the $\Delta(1232)$ as well as direct vector meson decays $\mathrm{V} \to \mathrm{e}^+\mathrm{e}^-$ with $\mathrm{V} = \rho, \omega$. The plain bremsstrahlung contribution is expected to be small at the present beam energy [27]. Similar cocktails have also been considered in previous attempts to describe the dielectron production in pp, pd and pA collisions [23,25, 28–34]. Schematically, the differential distribution of dielectrons with invariant mass M_{ee} can be expressed as a superposition of the above-mentioned decay channels

$$\frac{\mathrm{d}\sigma}{\mathrm{d}M_{ee}} = \sum_i \sigma_i \frac{\mathrm{d}\Gamma_i}{\Gamma_i^{tot}\mathrm{d}M_{ee}}\,. \tag{1}$$

This expression means that a parent hadron i is created in the p+p collision with cross-section σ_i and decays subsequently, thus generating the distribution $\mathrm{d}\Gamma_i/\mathrm{d}M_{ee}$. The factor $1/\Gamma_i^{tot}$ is the inverse of the total width of hadron i; together with the partial width for the dielectron decay channel it encodes the branching ratio. Broad resonances, such as the ρ and $\Delta(1232)$, are actually generated at masses m_ρ and m_Δ (see (2) below), and the decay distribution depends correspondingly on $m_{\rho,\Delta}$ and M_{ee} (cf. eqs. (20, 21) in [23]). Note that non-strange baryon resonances besides the $\Delta(1232)$ are not included in PYTHIA. Moreover, in the case of Dalitz decays, the mass dependence of the electromagnetic transition form factors should be considered. The mass dependences of the electromagnetic transition form factors for the π^0, η and ω mesons are parametrized in PLUTO [26] according to [32,35] in agreement with recent measurements [36,37]. The direct decays of vector mesons are treated within the VMD model [38], while the formulas for the pseudoscalar ($P = \pi^0$ or η) and vector meson Dalitz decays are adopted from [35,39]. The Dalitz decay of the $\Delta(1232)$ resonance is simulated using the expression for its differential decay rate from [39]. In these calculations, the N-Δ transition vertex is described by electric, magnetic and Coulomb form factors, corresponding to three independent helicity amplitudes [40]. As mentioned in the introduction, in the time-like region the q^2 dependence of the transition form factors is not measured yet. Therefore, we make an approximation by fixing the form factors at the photon point (real photons) using the measured radiative decay width of the $\Delta(1232)$ ($\Gamma_{\Delta\to N\gamma} = 0.61$–$0.7$ MeV) [32,41]. We further neglect the terms with the electric form factor, as the electric transition is much weaker than the magnetic one [42].

It should be further noted that in PYTHIA the ρ and $\Delta(1232)$ resonances are implemented with constant total widths around the resonance pole mass. This treatment is not precise enough outside the resonance pole. Therefore, following the prescription of [5,43], we generate masses of $\Delta(1232)$, ρ and ω states inside PYTHIA according to the relativistic Breit-Wigner distribution

$$A(M) = N\frac{2}{\pi}\frac{M^2\Gamma_{tot}(M)}{\left(M^2 - M_{pole}^2\right)^2 + \left(M\Gamma_{tot}(M)\right)^2}\,, \tag{2}$$

with mass-dependent total width $\Gamma_{tot}(M)$ in case of $\Delta(1232)$ and ρ, and a constant total width at the pole for the narrow ω meson state. This mass dependence of the total width in case of the $\Delta(1232)$ baryon resonance is calculated from its dominant decay channel into pion and nucleon final states with the cutoff parametrization of [44]

$$\Gamma_{tot}^{\Delta}(M) \simeq \Gamma_{\Delta\to\pi N} = \Gamma_{pole}\frac{M_{pole}}{M}\left(\frac{q}{q_{pole}}\right)^3\frac{\delta^2 + q_{pole}^2}{\delta^2 + q^2}\,, \tag{3}$$

where $\delta = 0.197$ GeV, M is the actual mass of the $\Delta(1232)$, M_{pole} is its pole mass and Γ_{pole} is its pole width[5]. Furthermore, q and q_{pole} denote the pion 3-momenta in the rest frame of the $\Delta(1232)$ with mass M and M_{pole}, respectively. In [16] the authors investigate the effect of different cutoff prescriptions [44,45], in particular on the dielectron spectra for high masses. The resulting uncertainties are larger than a factor of 3.

The mass dependence of the ρ total width is parametrized according to [23].

The normalization constant in eq. (2), N, is chosen such that $\int_{min}^{max} A(M)\mathrm{d}M = 1$, where max is fixed at 2 GeV and min is taken to be $2m_\pi$, $3m_\pi$ and $m_\pi + m_N$ for ρ, ω and $\Delta(1232)$, correspondingly.

In contrast to PYTHIA and HSD, the transport model UrQMD [34] uses a resonance (R) excitation mechanism for the production of particles via two-nucleon (N) reactions of the type $NN \to NR$, $NN \to RR$. Resonances with masses up to 2.2 GeV for the N^* and 1.95 GeV for the Δ are included [22]. The production matrix elements for resonances are obtained from the experimental data

[5] In this paper, units with $c = 1$ are used for the formulas.

on π, η and ρ production, when available. The probabilities for the resonances to decay into specific channels are then given by the corresponding known branching ratios. Even though in UrQMD the excitation of many baryon resonances are used, only the Dalitz decay of the $\Delta(1232)$ isobar is explicitly included. The e^+e^- contribution from decays of higher-lying resonances is included via their ρ decay branches (see table 3.4 in [22]). However, this approach leads to an overestimation of the e^+e^- production from the ρ decays. On the other hand, estimates of the e^+e^- yield from the Dalitz decays of higher resonances indicate smaller contribution as compared to the one from $\Delta(1232)$ and η decays for $M_{ee} < 0.55\,\mathrm{GeV}/c^2$ [46–48]. Dalitz decays of higher-lying baryon resonances have also been investigated in [12]. Checking the validity of this approach for describing the experimental data is a subject of ongoing HADES activities.

In general, the reaction $pp \to e^+e^- X$ is fully described by three independent degrees of freedom (neglecting the internal degrees of freedom, like helicity angles of virtual photons) which can be selected in a variety of ways. It is important that a given event generator describes the experimentally measured distributions in all degrees of freedom. Therefore we present here the comparison of pair invariant mass, transverse momentum and rapidity distributions to the corresponding distributions from simulated PYTHIA, UrQMD and HSD events as discussed above. In doing so, the acceptance matrices mentioned above are used, *i.e.* the comparison is performed inside the HADES acceptance. Furthermore, momenta of leptons are smeared in the simulation in order to take into account our finite detector resolution. The smearing functions are obtained by propagating simulated e^+ and e^- tracks through the detector setup using the Geant package [49,50], hence taking into account the interaction of leptons with the detector material as well. This is, in particular, visible in the simulated ω peak shape, where the tail towards low masses is due to the energy loss of electrons via electromagnetic radiation (bremsstrahlung). On the other hand, the ionization (collisional) energy loss of electrons shifts the pole position of the reconstructed omega peak by 1% downwards.

3.2 Invariant-mass distribution

The comparison of the experimentally measured invariant-mass distribution of e^+e^- pairs to the PYTHIA+PLUTO results is presented in fig. 2(a). The simulated cocktail (the sum of the different cocktail contributions is plotted as a green curve) reproduces results of GiBUU [25] and describes the data reasonably well except for the mass range around $0.55\,\mathrm{GeV}/c^2$ where the yield is underestimated. The latter deviation is not too surprising, as the virtuality of the photon $\gamma^* \to e^+e^-$ reaches quite high values, and therefore it is not guaranteed that the $\Delta(1232)$ form factors fixed at the photon point are still valid. Furthermore, contributions of higher Δ and N^* resonances are not included which might also lead to some deficit.

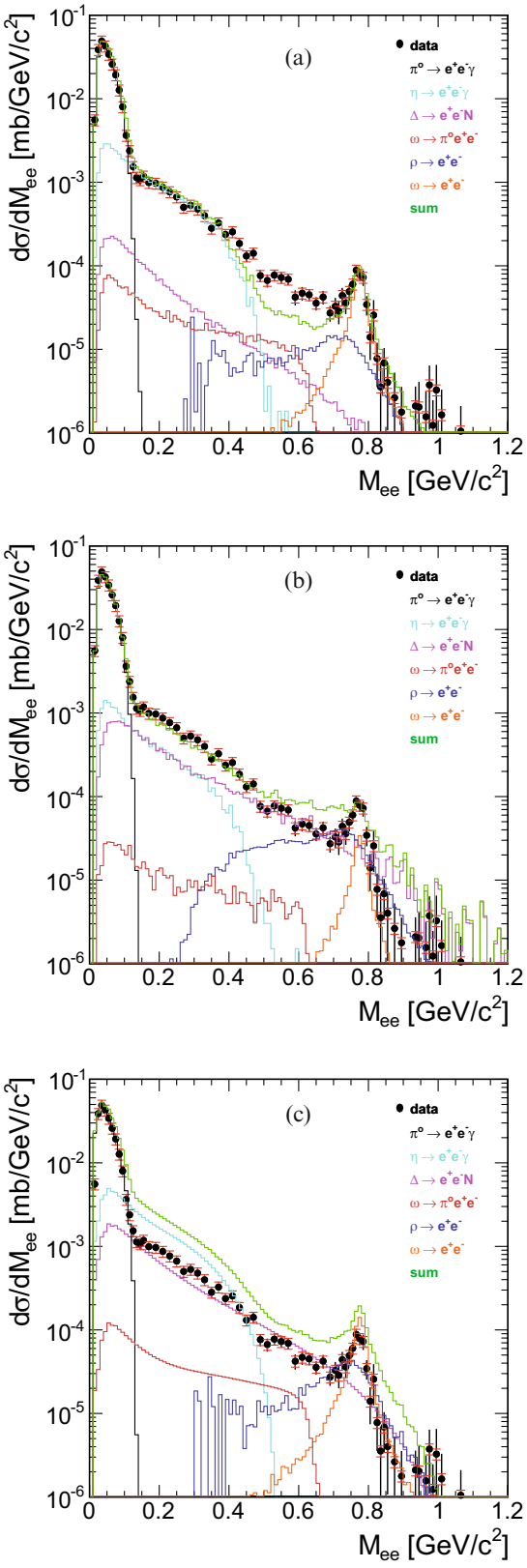

Fig. 2. (Color online) The HADES data for the p(3.5 GeV) + p $\to$ e^+ e^- X reaction, compared to a simulated cocktail from the a) PYTHIA, b) UrQMD and c) HSD event generators.

In fig. 2(b), we compare our results to the UrQMD [22] predictions. The simulated cocktail clearly overestimates the measurements at high masses. The strong ρ contribution might be due to the large $R \rightarrow N\rho \rightarrow N\mathrm{e}^+\mathrm{e}^-$ couplings as mentioned already above. Figure 2(c) illustrates the comparison of the same experimental data to the HSD results. In this case, the simulated cocktail has too strong contributions for all components, except the π^0. The comparison of figs. 2(a), (b) and (c) points to a lack of understanding of the relative strengths of the $\Delta(1232)$ and low-mass ρ contributions. For instance, as discussed in [4], implementation of the Iachello model [15] enhances dielectron yield in the high-mass region. This has also been demonstrated in [25,51]. We expect hence that our data can help to clarify the issue of form factors in the $\Delta(1232)$ Dalitz decay and the role of other baryon resonances, as mentioned in the introduction. The data may also serve as an important constraint for the possible quantum interference effects between ρ and ω mesons [52,53].

3.3 Transverse momentum distributions

The $\mathrm{e}^+\mathrm{e}^-$ pair transverse momentum p_t distributions for different invariant mass bins inside the acceptance of HADES are presented in figs. 3(a), (b), (c) and compared with the respective results from PYTHIA+PLUTO, UrQMD and HSD calculations. In the mass range $M_{\mathrm{e}^+\mathrm{e}^-}$ [GeV/c^2] < 0.15, dominated by the contribution from dielectrons stemming from the π^0 Dalitz decay, the experimental p_t distributions are in reasonable agreement with the simulated p_t distributions from PYTHIA. It should be emphasized that parameter PARP(91) (see table 1) steers essentially the transverse momentum distributions. The next mass range of $0.15 < M_{\mathrm{e}^+\mathrm{e}^-}$[GeV/$c^2$] < 0.47 constrains the cross-sections of the η meson and the $\Delta(1232)$ isobar. Again, tuned PYTHIA reproduces the experimental data, while UrQMD is low by a factor of 2 at low p_t and a factor of 5 too high at large p_t. In this mass interval, the low-p_t part of the spectra is populated mainly by the pairs originating from η Dalitz decays. It is therefore obvious that the UrQMD underestimates the contribution from the η meson. On the other hand, the high-p_t part contains, in addition, a substantial contribution from the $\Delta(1232)$ Dalitz decay, which in case of UrQMD is too strong. Thus, the transverse momentum distributions in suitable invariant-mass bins add important information on the various contributions. Indeed, an inspection of fig. 2(b) evidences that the sum of η and Δ contributions within UrQMD reproduces the invariant-mass distribution in the interval $0.15 < M_{\mathrm{e}^+\mathrm{e}^-}$ [GeV/c^2] < 0.47 fairly well, but fails in the transverse momentum distribution in corresponding mass bin (cf. fig. 3(b)).

The HSD results in this mass bin overestimate the experimental results by large factors at high p_t. In the mass interval of $0.47 < M_{\mathrm{e}^+\mathrm{e}^-}$ [GeV/c^2] < 0.7 the experimental data cannot be satisfactorily described by any of these models. The shape of the p_t distribution in the bin $M_{\mathrm{e}^+\mathrm{e}^-}$ [GeV/c^2] > 0.7, dominated by direct decays of the vector mesons, is nicely described by the tuned PYTHIA.

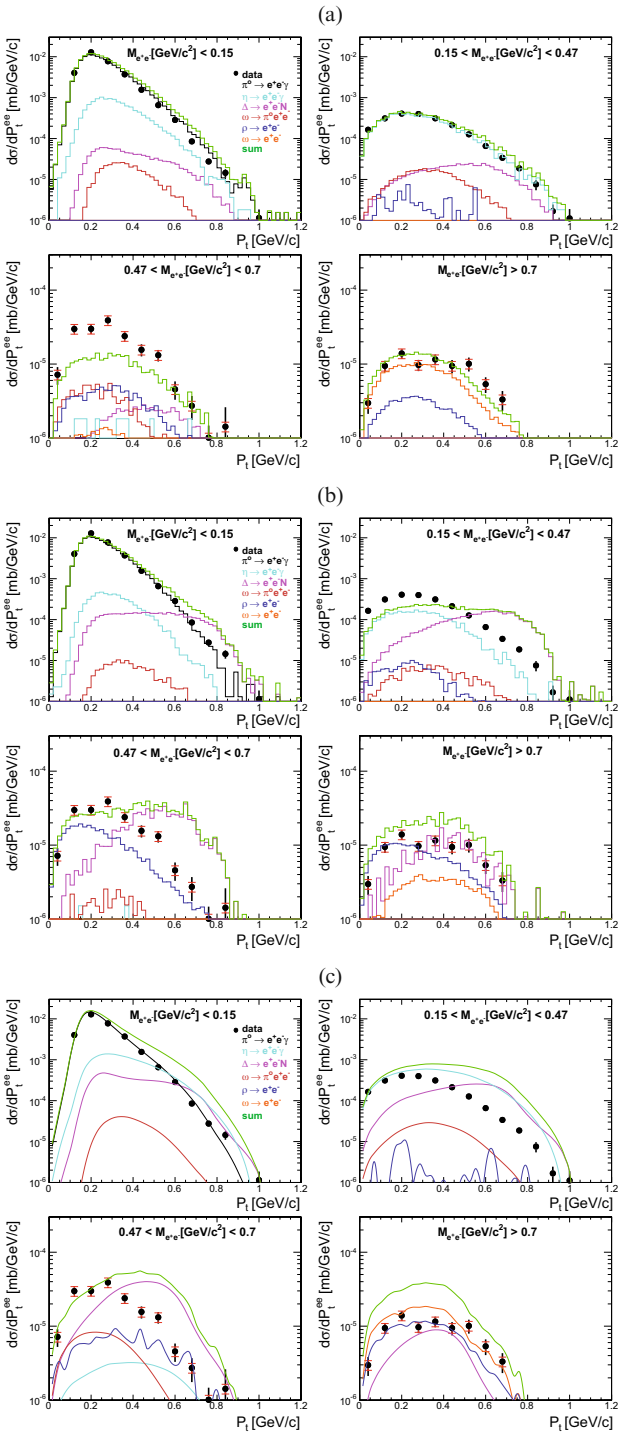

Fig. 3. (Color online) Comparison of experimental p_t distributions to the a) PYTHIA, b) UrQMD and c) HSD events for different $\mathrm{e}^+\mathrm{e}^-$ invariant-mass ranges as indicated.

Different shape of the ρ meson traverse momentum in UrQMD is just a phase-space effect due to is production through resonances. Presented transverse-mass distributions, in particular their slopes, are important constraints for particle productions in elementary reactions at this energy.

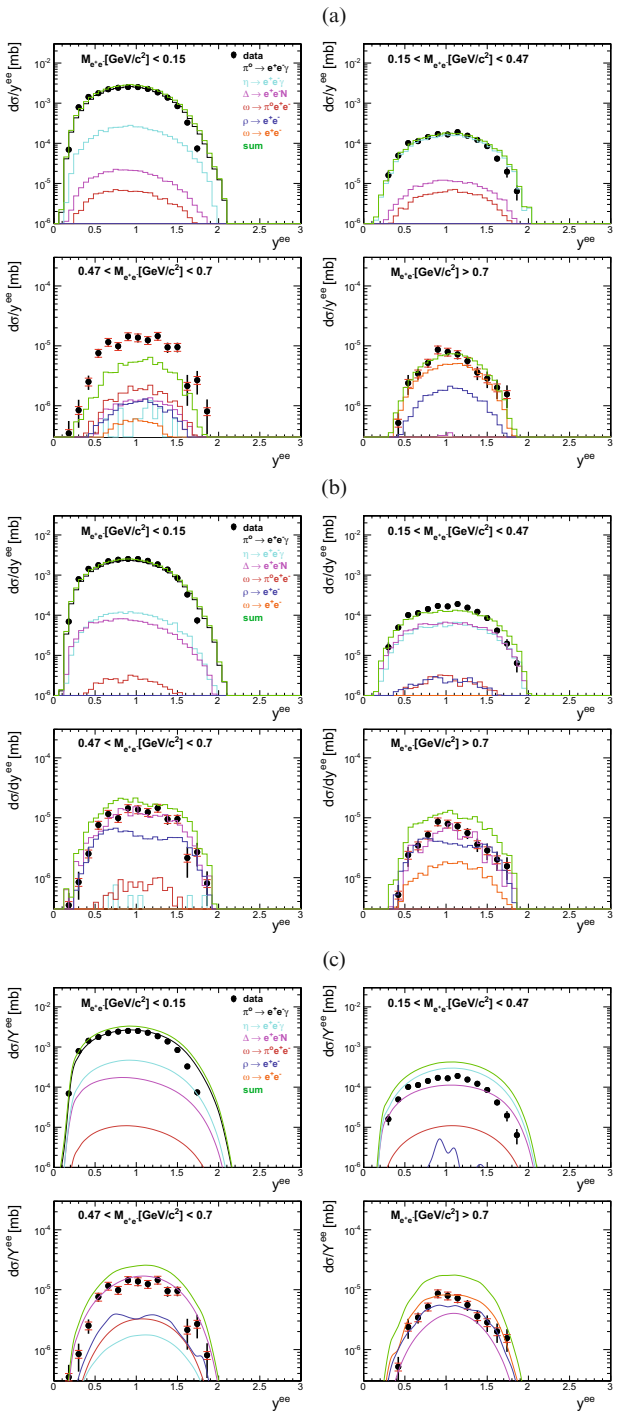

Fig. 4. (Color online) Comparison of experimental rapidity distributions to the a) PYTHIA, b) UrQMD and c) HSD event generators for different e^+e^- invariant-mass bins as indicated.

3.4 Rapidity distributions

In contrast to the p_t distributions, the rapidity distributions do not exhibit such large differences between the different models (see fig. 4). This may originate from the fact that the impact of the large-p_t region to these spectra is reduced due to the p_t integration in each rapidity bin.

4 Extraction of the π^0, η, Δ, ρ, and ω cross-sections

The inclusive cross-section of the neutral pion production inside the HADES acceptance was estimated from its Dalitz decay channel, $\pi^0 \rightarrow e^+e^-\gamma$, by integrating the measured yield in the mass interval between 0 and $0.15\,\mathrm{GeV}/c^2$ (see fig. 2(a)), and by correcting for the branching ratio $(1.198\pm0.032)\%$ [54]. This result is further extrapolated to full phase-space using a correction factor determined by filtering simulated events with the HADES acceptance matrices defined in sect. 2 and applying cuts used in the analysis of experimental data (*i.e.*, e^+e^- opening angle and lepton momentum cuts described in sect. 2). In order to account for dependency of the extrapolation factor on the assumed pion production mechanism, we have used an average factor extracted from calculations based on URQMD and PYTHIA events. Furthermore, from this simulations we have also derived a systematic error (see table 2) defined as the difference between both calculations. Finally, the extracted cross-section was corrected for the pions originating from the ω and η mesons decays.

The cross-section for the η mesons was obtained in a similar way but by integrating directly its contribution to the simulated cocktail presented in fig. 2(a), correcting for its Dalitz decay branching ratio $(7 \pm 0.7) \times 10^{-3}$ [54] and extrapolating to full phase-space. We have checked that the same result, within 3.7%, is obtained by extrapolation of the integrated experimental e^+e^- yield with subtracted contributions of other sources in the invariant-mass range of $0.15 < M_{e^+e^-}\ [\mathrm{GeV}/c^2] < 0.5$. The most important one originates from the $\Delta(1232)$ Dalitz decays[6]. We fixed the Δ production cross-section from our PYTHIA simulations reproducing the respective p_t distributions (see fig. 3(a)). The contribution from the ω Dalitz decay in this mass range is fixed by its known branching ratio and cross-section defined by its direct decay channel, as explained below. The model dependence of the extrapolation factor for the η meson was accounted for as for the pion. As one can see from table 2, the respective model errors for both mesons are small, though the PYTHIA and URQMD use quite different assumptions about the production mechanism of the mesons.

The production cross-sections for the vector mesons were obtained from their multiplicities in full phase-space generated by PYTHIA. This is motivated by the fact that the spectrometer acceptance in the respective mass and p_t range is high ($\sim 30\%$) and flat (see fig. 42 in [1]) and does not introduce any bias, as shown by dedicated simulations. The other errors quoted in table 2 are the results of statistical error propagation with the systematic one added in quadrature. The latter is stemming from the normalization to the elastic p+p cross-section and the efficiency correction procedure. Figure 5 shows a compilation of measured production cross-sections of vector mesons (ω, ρ) in p+p reactions at different energies. Similar plots for different pion species and the η meson are shown in fig. 6.

[6] Note that both, Δ^+ and Δ^0 states, are taken into account.

Table 2. Inclusive cross-sections obtained for different particles. For the π^0 and η mesons, we use the average values of the cross-sections obtained with PYTHIA and UrQMD extrapolations as explained in the text. The quoted errors are results of statistical error propagation with the systematic one added in quadrature. The systematic errors due to model dependence are quoted separately.

	π^0	η	$\Delta^{0,+}$	ρ	ω
σ_i [mb]:	$17 \pm 2.65 \pm 1$(model)	$1.035 \pm 0.17 \pm 0.105$(model)	7.5 ± 1.3	0.233 ± 0.06	0.273 ± 0.07

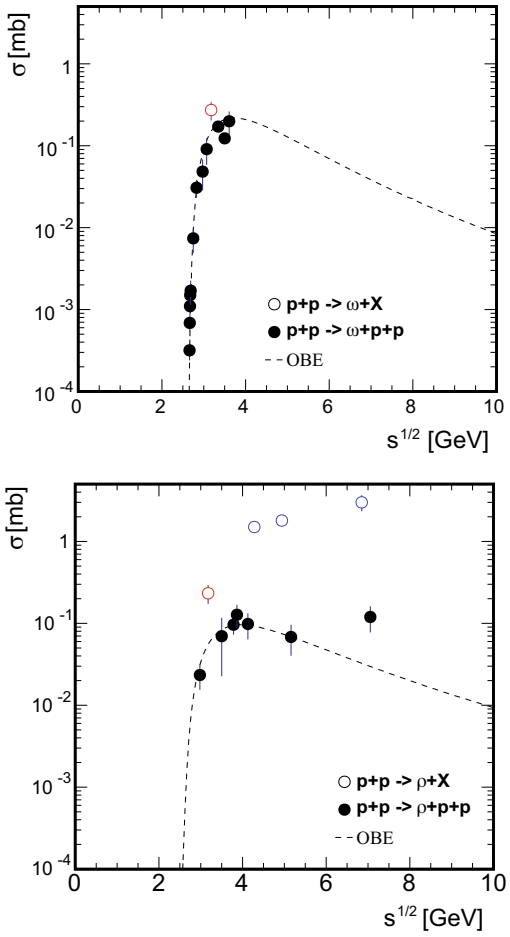

Fig. 5. (Color online) Cross-sections for the vector mesons ω (upper panel) and ρ (lower panel), in p+p collisions as a function of the Mandelstam variable s. Open circles represent the inclusive production cross-sections, while the full circles correspond to exclusive productions [55]. The dashed curve refers to the OBE calculations for the exclusive channels [56]. The cross-section values obtained in this work are depicted in red.

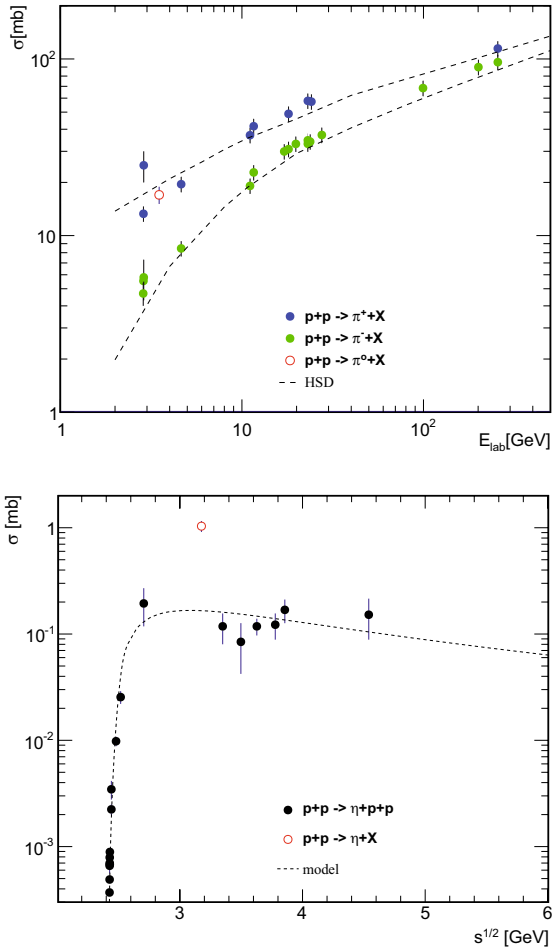

Fig. 6. (Color online) Cross-sections of pions (upper panel) and η mesons (lower panel) in p+p interactions [55,57–61]. The dashed lines in the case of pions refer to the parametrizations used in the HSD transport model, while for the η meson the line corresponds to its exclusive production through the $N^*(1535)$ resonance [62]. The full circles, in this case, illustrate the measured exclusive production cross-sections of the η mesons in p+p collisions. The inclusive production cross-section values obtained in this work are depicted with red open circles.

5 Direct decays of the η meson

Using the data described above we can derive an upper limit for the branching ratio of the direct η meson decay $\eta \rightarrow e^+e^-$. Figure 7 shows the invariant-mass distribution of the e^+e^- pairs in the η meson mass range. The experimental data points are fitted with a polynomial background function, excluding some range around the η meson mass. There is no visible indication of a peak structure from the direct decays of η mesons. Indeed, performing the Kolmogorov-Smirnov test one gets a 90% probability for the consistency of the background function and the data points. However, one can still estimate an upper limit for this decay process from the data using the method of

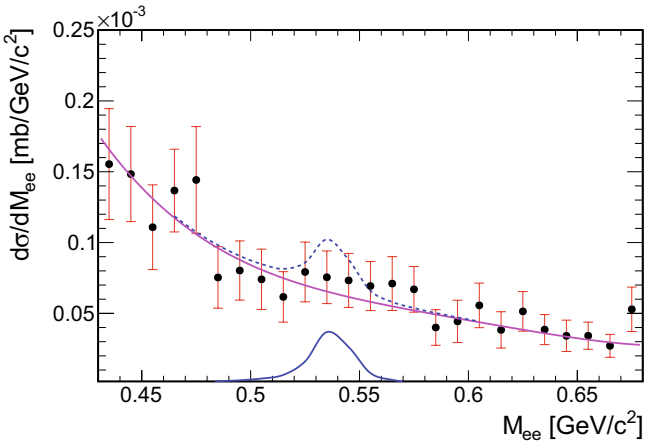

Fig. 7. (Color online) Invariant-mass distribution of e^+e^- pairs in the η meson mass range. The experimental data is fitted with a polynomial distribution (magenta curve) by excluding the range of $m_\eta \pm 3\sigma$ around η meson pole mass. The invariant-mass distribution of e^+e^- pairs from simulated direct dielectron decays of the η meson (blue curve) is presented on top of the background (dashed blue curve).

Feldman and Cousins [63]. In order to test the robustness of the obtained results, five different ranges of the background function have been tested. Moreover, the same procedure was repeated for different polynomial functions. The output of the Feldman Cousins method is an upper limit for the signal counts with a 90% confidence level. Using this upper limit for the signal counts and the η production cross-section, reported in the previous section, an upper limit for the branching ratio of $(4.9{+}0.7{-}1.2){\times}10^{-6}$ is obtained. This value is about 6 times lower than the most recent value of 2.7×10^{-5} from [64]. To demonstrate how the hypothetical η peak would look like, we show in fig. 7 the η shape from a simulation on top of the experimental data, using the branching ratio of 4.9×10^{-6} and the production cross-section of 1.035 mb from table 2. The significance of the added hypothetical peak amounts to 5%.

6 Summary

In summary, we reported on a dielectron measurement in p+p collisions at 3.5 GeV projectile kinetic energy. For the first time the inclusive production cross-sections for neutral pions, η, ω and ρ mesons were determined from dielectron experimental data. The experimental distributions were compared to the results from the PYTHIA, UrQMD and HSD event generators, which use different physics assumptions to generate the parent hadrons decaying subsequently into e^+e^- at this projectile energy. With some minor tunes, PYTHIA+PLUTO results describe the experimentally observed distributions in a better way than the resonance production picture used in UrQMD. We hope that our data stimulate further work pinning down the issue of form factors in $\Delta(1232)$ Dalitz decays and shed light on the role of other baryon resonances in p+p collisions. Using our data, it was demonstrated that the upper bound for the direct $\eta \to e^+e^-$ decay can be improved by a factor of ∼6 compared to the value quoted in [64].

We would like to thank our theory colleagues, especially E. Bratkovskaya, J. Weil, E. Santini, M. Bleicher and G. Wolf for useful discussions and suggestions. The Collaboration gratefully acknowledges the support by LIP Coimbra, Coimbra (Portugal): PTDC/FIS/113339/2009, SIP JUC Cracow, Cracow (Poland): N N202 286038 28-JAN-2010 NN202198639 01-OCT-2010, FZ Dresden-Rossendorf (FZD), Dresden (Germany): BMBF 06DR9059D, TU Munchen, Garching (Germany) MLLMunchenDFG EClust: 153VH-NG-330, BMBF 06MT9156 TP5 TP6, GSI TMKrue 1012, NPI AS CR, GSI TMFABI 1012, Rez, Rez (Czech Republic): MSMT LC07050 GAASCR IAA100480803, USC - S. de Compostela, Santiago de Compostela (Spain): CPAN:CSD2007-00042, Helmholtz alliance HA216/EMMI.

Open Access This is an open access article distributed under the terms of the Creative Commons Attribution License (http://creativecommons.org/licenses/by/3.0), which permits unrestricted use, distribution, and reproduction in any medium, provided the original work is properly cited.

References

1. HADES Collaboration (G. Agakichiev *et al.*), Eur. Phys. J. A **41**, 243 (2009).
2. S. Leupold, V. Metag, U. Mosel, Int. J. Mod. Phys. E **19**, 147 (2010).
3. R. Rapp, J. Wambach, H. van Hees, arXiv:0901.3289v1 [hep-ph] (2009).
4. HADES Collaboration (G. Agakichiev *et al.*), Phys. Lett. B **690**, 118 (2010).
5. HSD, `http://fias.uni-frankfurt.de/~brat/hsd.html`.
6. O. Buss *et al.*, arXiv:1106.1344v1 [hep-ph] (2011).
7. B. Andersson *et al.*, Phys. Rep. **97**, 31 (1983).
8. UrQMD, `http://urqmd.org`.
9. J.J. Sakurai, Ann. Phys. **11**, 1 (1960).
10. J.J. Sakurai, *Currents and mesons* (University of Chicago Press, Chicago, 1969).
11. N.M. Kroll, T.D. Lee, B. Zumino, Phys. Rev. **157**, 1376 (1960).
12. M.I. Krivoruchenko *et al.*, Ann. Phys. **296**, 299 (2002).
13. F. Iachello, A.D. Jackson, A. Lande, Phys. Lett. B **43**, 191 (1973).
14. F. Iachello, Q. Wan, Phys. Rev. C **69**, 055204 (2004).
15. Q. Wan, F. Iachello, Int. J. Mod. Phys. A **20**, 1846 (2005).
16. H.W. Barz, B. Kämpfer, Gy. Wolf, M. Zétényi, Open Nucl. Part. Phys. J. **3**, 1 (2010).
17. HADES Collaboration (A. Rustamov *et al.*), AIP Conf. Proc. **1257**, 736 (2010).
18. HADES Collaboration (G. Agakichiev *et al.*), Phys. Lett. B **663**, 43 (2008).
19. HADES Collaboration (G. Agakichiev *et al.*), Phys. Rev. Lett. **98**, 052302 (2007).
20. R.C. Kammerud *et al.*, Phys. Rev. D **4**, 5 (1971).
21. PYTHIA, `http://home.thep.lu.se/~torbjorn/Pythia.html`, `arXiv:hep-ph/0603175v2`.

22. S.A. Bass *et al.*, Prog. Part. Nucl. Phys. **41**, 255 (1998).
23. E.L. Bratkovskaya, W. Cassing, Nucl. Phys. A **807**, 214 (2008).
24. K. Gallmeister, U. Mosel, Nucl. Phys. A **826**, 151 (2009).
25. J. Weil *et al.*, PoS **BORMIO2011**, 053 (2011) arXiv:1105.0314 [nucl-th].
26. I. Fröhlich *et al.*, arXiv:0708.2382v2 [null-ex].
27. L.P. Kaptari, B. Kämpfer, Nucl. Phys. A **764**, 338 (2006).
28. M. Schäfer, T.S. Biro, W. Cassing, U. Mosel, Phys. Lett. B **221**, 1 (1989).
29. B. Kämpfer, A.I. Titov, E.L. Bratkovskaya, Phys. Lett. B **301**, 123 (1993).
30. M. Schäfer, H.C. Dönges, A. Engel, U. Mosel, Nucl. Phys. A **575**, 429 (1994).
31. B. Kämpfer, A.I. Titov, E.L. Bratkovskaya, Phys. Rev. C **51**, 227 (1995).
32. C. Ernst *et al.*, Phys. Rev. C **58**, 447 (1998).
33. M. Thomère, C. Hartnack, G. Wolf, J. Aichelin, Phys. Rev. C **75**, 064902 (2007).
34. K. Schmidt *et al.*, Phys. Rev. C **79**, 064908 (2009).
35. L.G. Landsberg, Phys. Rep. **128**, 301 (1985).
36. NA60 Collaboration (R. Arnaldi *et al.*), Phys. Lett. B **677**, 260 (2009).
37. H. Berghäuser *et al.*, Phys. Lett. B **701**, 562 (2011).
38. G.Q. Li, C.M. Ko, G.E. Brown, H. Sorge, Nucl. Phys. A **611**, 539 (1996).
39. M. Krivoruchenko, A. Fässler, Phys. Rev. D **65**, 017502 (2001).
40. H.F. Jones, M.D. Scadron, Ann. Phys. **81**, 1 (1972).
41. I. Fröhlich *et al.*, Eur. Phys. J. A **45**, 401 (2010).
42. M. Gourdin, Ph. Salin, Nuovo Cimento **27**, 193 (1962).
43. E.L. Bratkovskaya, private communications.
44. D.M. Manley, E.M. Saleski, Phys. Rev. D **45**, 11 (1991).
45. J.H. Koch, E.J. Moniz, N. Ohtsuka, Ann. Phys. **154**, 99 (1984).
46. R. Shyam, U. Mosel, Phys. Rev. C **67**, 065202 (2003).
47. M. Zétényi, Gy. Wolf, Phys. Rev. C **67**, 044002 (2003).
48. M. Zétényi, Gy. Wolf, Acta. Phys. Hung. A **22**, 239 (2005).
49. HGEANT, `http://www-hades.gsi.de`.
50. GEANT 3.21, `http://consult.cern.ch/writeup/geant`.
51. HADES Collaboration (A. Rustamov *et al.*), *GSI Scientific report* (2010).
52. A.I. Titov, B. Kämpfer, Eur. Phys. J. A **12**, 217 (2001).
53. M. Lutz, B. Friman, M. Soyeur, Nucl. Phys. A **713**, 97 (2003).
54. K. Nakamura *et al.*(Particle Data Group), J. Phys. G **37**, 075021 (2010).
55. H. Schopper (Editor), in *Landolt-Börnstein, New Series*, Vol. **I/12** (Springer, Berlin, 1988).
56. A. Sibirtsev, W. Cassing, U. Mosel, Z. Phys. A **358**, 357 (1997).
57. M. Antinucci *et al.*, Lett. Nuovo Cimento **6**, 121 (1973).
58. NA49 Collaboration (J. Bächler *et al.*), Nucl. Phys. A **661**, 45 (1999).
59. E. Chiavassa *et al.*, Phys. Lett. B **332**, 270 (1994).
60. A.M. Bergdolt *et al.*, Phys. Rev. D **48**, 7 (1993).
61. H. Calen *et al.*, Phys. Lett. B **366**, 39 (1996).
62. S. Teis *et al.*, Z. Phys. A **356**, 421 (1997).
63. G.J. Feldman, R.D. Cousins, Phys. Rev. D **57**, 3873 (1998).
64. CELSIUS/WASA Collaboration (M. Berlowski *et al.*), Phys. Rev. D **77**, 032004 (2008).